Two-step growth procedure for homogeneous GaN NW arrays on graphene

Dyhia Tamsaout, Edmond Cambril, Laurent Travers, Ali Madouri, Noëlle Gogneau, Maria Tchernycheva, Jean-Christophe Harmand, Ludovic Largeau

Two-step growth procedure for homogeneous GaN NW arrays on graphene

Dyhia Tamsaout, Edmond Cambril, Laurent Travers, Ali Madouri, Noelle Gogneau, Maria Tchernycheva, Jean-Christophe Harmand[*]*, Ludovic Largeau*

Centre de Nanoscience et Nanotechnologie (C2N), Université Paris-Saclay, CNRS, 91120 Palaiseau, France

[*] *Corresponding author: jean-christophe.harmand@cnrs.fr*

Keywords: GaN, Nanowires, Molecular beam epitaxy, Electron-beam lithography, Selective area growth, Incubation.

ABSTRACT: Growth of GaN nanowires on graphene substrates is carried out by plasma-assisted molecular beam epitaxy. We test a two-step growth procedure consisting of a first stage at relatively low temperature followed by a second stage at higher temperature. We investigate the impact of this process on the usually long incubation time which precedes the first GaN nucleation events on graphene. We also examine how the selectivity of growth between graphene and the surrounding SiO_2 surface is affected. After optimization of this procedure, it is applied to the growth of GaN nanowires on a graphene layer patterned by electron beam lithography. A clear advantage of the two-step growth is observed in terms of reduction of the incubation time and improvement of height uniformity.

ABSTRACT: Growth of GaN nanowires on graphene substrates is carried out by plasma-assisted molecular beam epitaxy. We test a two-step growth procedure consisting of a first stage at relatively low temperature followed by a second stage at higher temperature. We investigate the impact of this process on the usually long incubation time which precedes the first GaN nucleation events on graphene. We also examine how the selectivity of growth between graphene and the surrounding SiO_2 surface is affected. After optimization of this procedure, it is applied to the growth of GaN nanowires on a graphene layer patterned by electron beam lithography. A clear advantage of the two-step growth is observed in terms of reduction of the incubation time and improvement of height uniformity.

Introduction

III-nitride nanowires (NWs) are promising nanomaterials for many optoelectronic applications, in particular for light-emitting diodes [1], [2]. They are highly sought-after owing to their wide band gap, enabling tunability across the entire visible spectrum and in the ultraviolet range. Improving their characteristics via crystal growth optimization is crucial for advancing optoelectronic and electronic devices. The use of a low-cost substrate is also highly desirable. The growth of GaN NW has been

investigated on several substrates under various conditions and by different techniques such as metalorganic chemical vapor deposition [3], hydride vapor phase epitaxy [4] or plasma-assisted molecular beam epitaxy (PA-MBE). The later technique has proved to be effective in obtaining high quality GaN NWs [5]. However, with this growth technique, it has been observed that a long incubation time, typically several tens of min, precedes the nucleation of the first GaN islands before full NW development. This has been reported on Si (111) with or without AlN buffer layer [6], [7], [8], amorphous Al_xO_y [9] or SiN_x [10], and graphene [11]. This long incubation period means that an excess of source material is consumed and the process takes longer. Moreover, nucleation events can be widely distributed over time, around and after the mean incubation time, leading to a dispersion of NW lengths at the end of growth. An important challenge is thus to minimize the incubation time which is detrimental from the point of view of GaN NW growth efficiency and uniformity. Several studies have been carried out in this field, exploring various methods to accelerate the nucleation and promote uniform growth. These approaches include the pre-deposition of an AlN buffer layer [8] or catalyst particles [12], the reduction of growth temperature and the increase of the incoming N and Ga fluxes [10], [11], [13].

As previously shown, GaN NWs can be epitaxially grown on a single graphene layer [14]. Under certain conditions, the growth which was also performed by PA-MBE, was found highly selective with respect to silica onto which the graphene flakes were transferred. Graphene on an amorphous carrier material is therefore an original and promising alternative to bulk crystalline substrates for the epitaxial growth of high quality GaN nanostructures, in particular for the development of flexible devices, since graphene films can be transferred onto almost any support. In addition, with a graphene substrate, the difficulties associated with mismatches in lattice parameters and thermal expansion coefficients between the substrate and epi-material are reduced. However, as observed with other substrates, GaN NW growth on graphene does not start before a long delay of exposure to the Ga and N fluxes. A priori, nucleation on graphene is even more difficult than on more conventional substrates because this two-dimensional material has no dangling bonds at its surface of low energy. The incubation time determined by reflection high energy electron diffraction (RHEED) on the sample surface, reaches 90 min under standard conditions at a substrate temperature of 815°C and from the beginning of the exposure of graphene to the atomic fluxes [11]. It has been shown that during this long delay, the exposure to N and Ga fluxes modifies the graphene layer by incorporation of N atoms into pyridine sites. This stage was found necessary to trigger GaN nucleation and eventually form NWs.

A straightforward approach to reduce the incubation time, τ_i, is to lower the growth temperature, T_g. Indeed τ_i increases exponentially with T_g [7], [10], [11]. However, our final aim is to fabricate organized arrays of GaN NWs by patterning the graphene layer and exploiting the growth selectivity between graphene and the underlying SiO_2 carrier layer. This selectivity is perfect at $T_g = 815°C$ but it degrades rapidly for lower temperatures, nucleation becoming possible on SiO_2 (note that the longitudinal axis of NWs grown on amorphous SiO_2 deviates from perfect vertical alignment by a few degrees on average [15]). The reduction of T_g is also detrimental for the optical quality of the NWs [16]. Then a compromise must be found or an alternative growth strategy must be implemented to reduce the incubation time while preserving the growth selectivity as well as a high optical quality. An attractive strategy is to use a two-step growth procedure. Zettler *et al.* explored such a growth procedure on Si (111), consisting in an initial step at low temperature to promote rapid nucleation and a second step at higher temperature to elongate the NWs[8]. In the present study, we investigate a similar strategy for GaN NW grown on graphene. The two-step procedure is optimized on large graphene patches transferred on amorphous SiO_2 and then applied to samples with graphene patches pre-patterned at the nm scale by electron-beam lithography.

Methods

The graphene-on-silica substrates are prepared by wet transfer. We use a 1 cm^2 polycrystalline monolayer of graphene grown by chemical vapor deposition on a copper foil. The size of the graphene grains is a few tens of µm. We transfer this monolayer onto a 300-nm-thick amorphous SiO_2 carrier layer obtained by thermal oxidation of an n-type Si (100) substrate (see supplementary information). The size of the carrier substrate is a quarter of a two-inch wafer. In the MBE chamber, T_g was measured by an optical pyrometer calibrated before each run, by observing the (1 × 1) to (7 × 7) surface reconstruction transition on Si (111), which occurs at 860 °C. Prior to the growth, the substrate was outgassed at 850°C for 15 min to remove residual impurities from the surface. Then the substrate was exposed to a Ga flux equivalent to a planar GaN growth rate of 0.62 monolayer/s (9.6 nm/min) and to an active N flux corresponding to a N/Ga ratio in the vapor phase of 1.1. Our standard T_g is 815°C, temperature for which growth selectivity is perfect. The incubation time is determined by detecting the first GaN-related diffraction spots in the RHEED pattern. After growth, the samples are observed by scanning electron microscopy (SEM) and transmission electron microscopy (TEM) to analyze the geometrical and structural characteristics and the surface densities of the NWs. The nanowires have a hexagonal crystalline structure and grow along their $[000\bar{1}]$ axis by a vapor-solid mechanism as suggested by the absence of any particle at their top facet (see supplementary information, figure S1). The SEM images have been obtained by collecting the secondary electrons with a through lens detector (TLD) biased at +70 V and a working distance of 4.2 mm. The TLD is mounted out of the optical axis leading to a topographical contrast in the image. The SEM images are processed and analyzed using ImageJ software.

Results

A first series of experiments was carried out to evaluate the shortening of τ_i by reducing T_g. We recall that for our standard T_g of $815°C$, we are measuring a particularly long τ_i of $90\ min$. By using a growth temperature of $785°C$, we reduced the incubation period to $15\ min$, after which effective growth was performed for $20\ min$. Fig. 1a reveals that in this sample, NW formation exclusively occurs on the SiO_2 layer and not on the graphene substrate. This means that our determination of τ_i by RHEED at this reduced temperature corresponds to the initiation of NW nucleation on the SiO_2 surface around the graphene patch, but not on graphene itself. In other words, at $T_g = 785°C$, the energy barrier for nucleation on oxide becomes lower than that on graphene. This growth temperature is therefore not suitable for our purpose. Fig. 1b shows a sample of GaN NWs grown at $T_g = 795°C$. The incubation time was $25\ min$ and effective growth was performed for further $20\ min$. The NWs are present on both oxide and graphene, but their density is greater on graphene than on SiO_2, meaning that growth took place preferentially but not selectively on graphene. Finally, Fig. 1c shows a sample of GaN NWs grown at $T_g = 800°C$. We measured $\tau_i = 40\ min$ and set $30\ min$ of effective growth time. With these conditions, growth selectivity was perfectly recovered since NWs are present only on graphene.

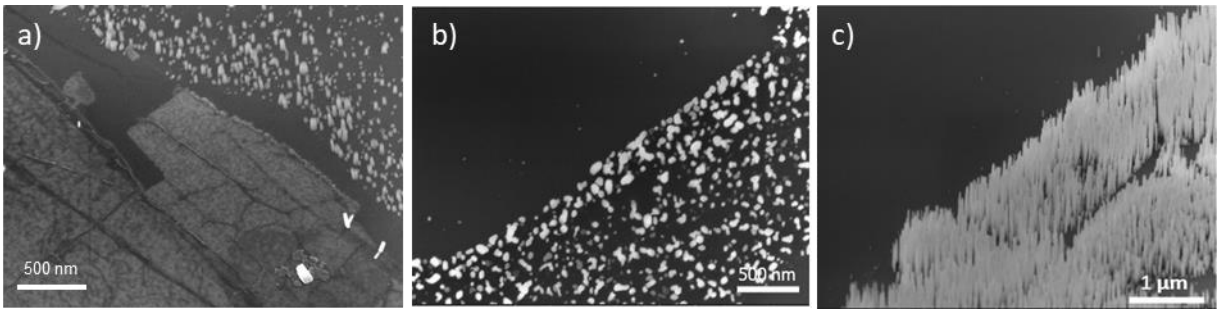

Figure 1 : Selectivity of GaN nanowire growth between SiO_2 (upper region) and graphene (lower region) areas at different growth temperatures observed by SEM: a) $T_g = 785°C$; b) $T_g = 795°C$; c) $T_g = 800°C$.

The results of this first series of samples were used to establish the conditions of a two-step growth procedure. The first growth step must result in the reduction of the incubation time on graphene but it must not lead to nucleation on SiO_2. Its temperature, T_{g1} cannot be set at $785°C$ because we have seen that the energy barrier for nucleation on oxide becomes lower than that on graphene at this temperature. If we set $T_{g1} = 795\ °C$, the duration of the first step, t_1, must be longer than the $25\ min$ of incubation and shorter than $45\ min$. Indeed these $45\ min$ correspond to an effective growth time of $20\ min$ which has resulted in the presence of NWs on both graphene and SiO_2. Using a temperature T_{g1} of $800°C$ would ensure selective growth but at the expense of a longer incubation time. Therefore, we selected the condition $t_1 = 35\ min$ in order to avoid parasitic NWs growing on SiO_2. For the second growth step, we tested three different growth temperatures T_{g2}, equal to $815°C$, $825°C$ and $835°C$. The duration of this second step, t_2, was fixed at $90\ min$. Ga and N fluxes remained unchanged throughout the experiments. In the following, the samples will be referred to as A, B and C, for T_{g2} equal to $815°C, 825°C$ and $835°C$, respectively. We also grew a reference sample in a single growth step which was identical to the first growth step of samples A, B and C.

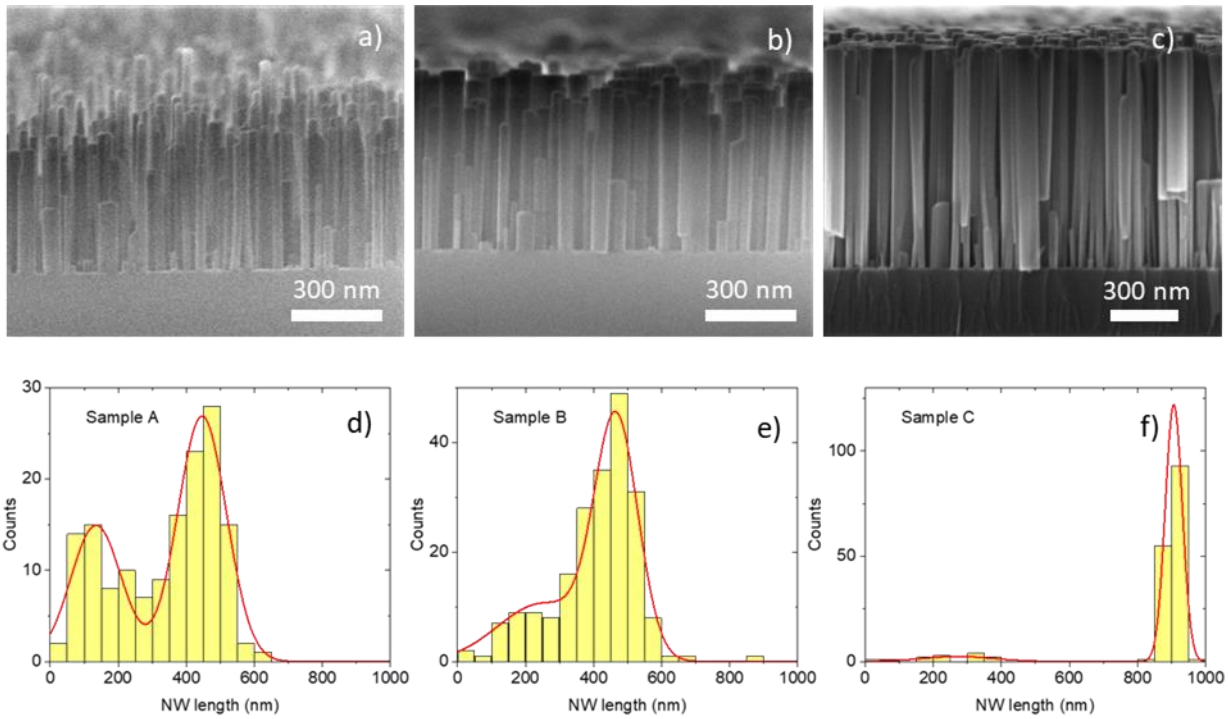

Figure 2: Cross-sectional SEM image (a, b, c) and height distribution (d, e, f) of GaN nanowires on graphene grown in two-step process. First step $t_1 = 35\ min$ at $T_{g1} = 795°C$, second step $t_2 = 90\ min$ at $T_{g2} = 815°C$ for sample A (a, d), at $T_{g2} = 825°C$ for sample B (b, e), at $T_{g2} = 835°C$ for sample C (c, f). Note that the scale range of the NW length axis is the same for the three samples.

The SEM images of samples A (Fig. 2a), B (Fig. 2b) and C (Fig. 3c) reveal that the uniformity of NW lengths varies significantly from sample to sample. A strong length dispersion is observed for $T_{g2} = 815°C$, it reduces for $T_{g2} = 825°C$, and a good length uniformity is obtained at $T_{g2} = 835°C$. To quantify this observation, we present the length distribution measured for several hundreds of NWs on each sample (Fig. 2d, 2e, 2f). At $T_{g2} = 815°C$, we identify two populations of NWs in terms of length: a short population with lengths distributed around $135\ nm$ and a longer population with lengths distributed around $450\ nm$ (Fig. 2d). In this sample, the population of long NWs is the largest (population ratio is 1.8). In sample B for which $T_{g2} = 825°C$, two populations of NWs are still observed (Fig. 2e) and their ratio is largely in favour of the longer ones (population ratio is 2.0). In sample C with $T_{g2} = 835°C$, the length distribution of the longer population is very narrow (Fig. 2f) and the short NWs have almost disappeared (population ratio is 11.9).

This first statistical analysis based on SEM cross-section images could be slightly flawed because a part of short NWs is hidden by the highest ones on these images. For this reason, we carried out another analysis based on SEM top views of the same three samples (Fig. 3) and of the reference sample (Fig. 4). In all these samples, the NW top facets present various SEM contrasts. Since the images are collected using out-of-axis TLD, the brighter top facets correspond to the longest NWs. Conversely, the top facets of lower intensities correspond to shorter NWs (see supplementary information). Although we did not establish the exact correspondence between the height of a particular NW and the brightness of its top facet, this second analysis is probably more viable than the one based on cross-section views for numbering populations of different heights.

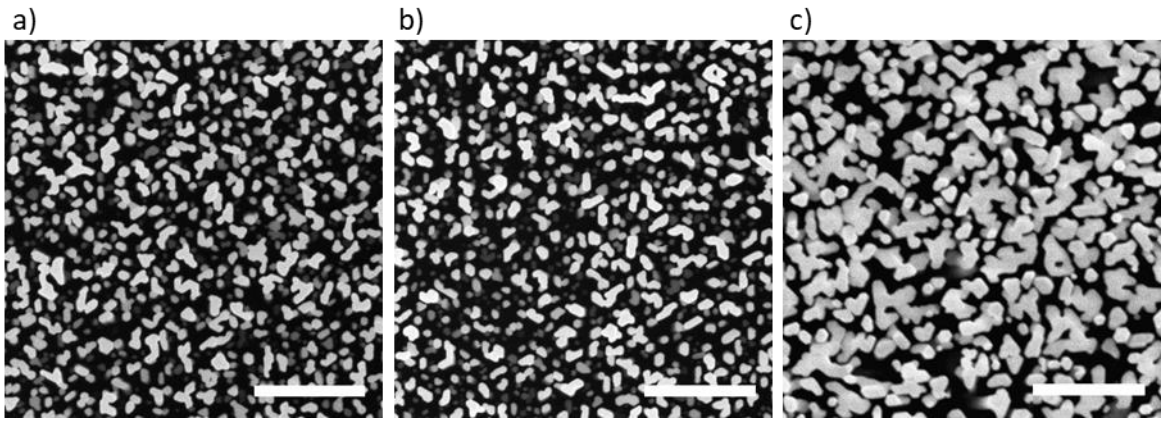

Figure 3: Top-view SEM images of samples grown in a two-step process: a) sample A, $T_{g1} = 795°C$ and $T_{g2} = 815°C$; b) sample B, $T_{g1} = 795°C$ and $T_{g2} = 825°C$; c) sample C, $T_{g1} = 795°C$ and $T_{g2} = 835°C$. Scale bars: 500 nm.

Furthermore, the SEM top views of Fig. 3 also reveal frequent coalescences of NWs, which are particularly apparent in the sample with $T_{g2} = 835°C$ (Fig. 3c). These coalescences complicate the precise numbering of individual NWs of a given range of top facet intensity. To determine and take into account the coalescence of two or more NWs, we used a method proposed by Brandt and co-workers [17]. These authors measured the circularity of the top facet of objects resulting from the coalescence of several NWs. The circularity is defined as $C = 4\pi A/p^2$where A is the area of the cross section of the object and p its perimeter. Indeed, individual NWs exhibit a shape resembling a regular hexagon, with a circularity slightly less than 1 (0.907). When two NWs coalesce, the shape of

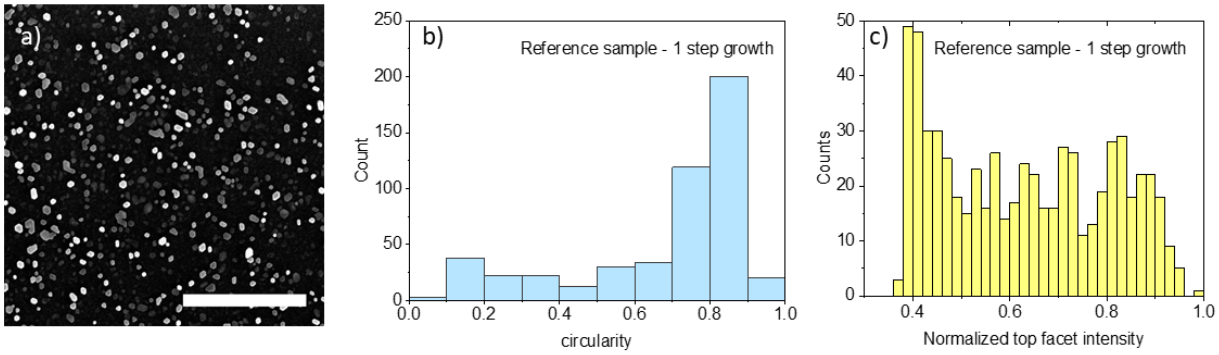

Figure 4: Characteristics of the reference sample grown in a single step. a) SEM top view with a scale bar of 500 nm; b) histogram of circularities of the top facets; c) histogram of intensities of the top facets.

the resulting object deviates from that of a regular hexagon, leading to a reduction in their circularity. For instance, two regular hexagones sharing one of their sides have a circularity of 0.653. Generally, when coalescence involves more than two NWs, the circularity continues to decrease. Of course, this statement is not always verified and can be contradicted by certain configurations of coalescence. Moreover, the lateral growth which may happen after coalescence can minimize the decrease of circularity. Nevertheless, we use a rule that follows a trend based on the circularities of regular and connected hexagons to estimate how many NWs have formed a particular object by coalescence: we have considered that circularities higher than 0.75 correspond to single NWs, circularities between 0.6 and 0.75 correspond to coalescence of two NWs; C between 0.5 and 0.6, 0.43 and 0.5, 0.38 and 0.43

are associated to 3 , 4 and 5 NWs, respectively (see supplementary information). We measured the circularity of the various objects observed in the top-view SEM images of our samples. Areas of about $5\ \mu m^2$ were analyzed for each sample. The histograms of circularity are presented in Fig. 5 for the double-step growth samples.

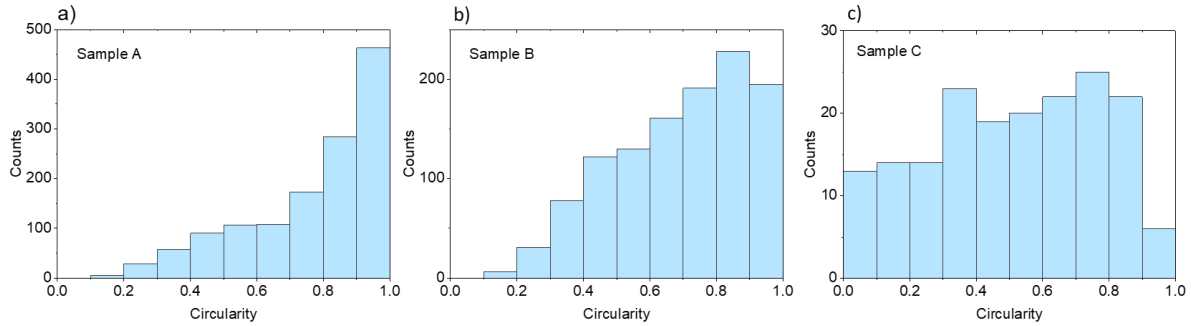

Figure 5: Circularity distribution for the ensembles of objects identified on samples grown in a two-step process. a) sample A, $T_{g1} = 795°C$ and $T_{g2} = 815°C$; b) sample B, $T_{g1} = 795°C$ and $T_{g2} = 825°C$; c) sample C, $T_{g1} = 795°C$ and $T_{g2} = 835°C$.

In sample A (Fig. 5a), the majority of objects (66 %) exhibit circularities greater than 0.75, indicating a limited degree of coalescence. In sample B (Fig. 5b), a significant reduction of circularities above 0.75 is observed (46 % of the objects), suggesting an increasing degree of coalescence. Finally, sample C (Fig. 5c) shows a very high degree of coalescence. This is obvious in the SEM image (Fig. 3c) which shows top facets of very large areas. Some of them are several tens of times larger than the average top-facet area of single non-coalesced NWs. Compared with these samples grown in two stages, the reference sample has a circularity distribution (Fig. 4b) indicating a small number of coalescence events. Therefore, coalescence is probably favored by significant radial growth during the second growth step. Our data suggest that this radial growth is most significant at the highest temperature of the second growth step. This tendency is also revealed by extracting, for each sample, the average diameter of the non-coalesced NWs from our data. For the reference sample obtained with a single growth step, this average diameter is $25.0\ nm$. It increases to $28.4\ nm$ in sample A, $32.8\ nm$ in sample B and $44.6\ nm$ in sample C.

We now return to our considerations on the SEM contrast. For each object, we calculate its normalized intensity as $I_n = (I - I_0)/(I_{max} - I_0)$ where I is the average intensity of the pixels of its top facet, I_0 the background intensity and I_{max} the average intensity of the brightest top facet of the image. The objects are then distributed according to their degree of coalescence, as defined by the simple rule given above. This partition being established, we extract the actual number of NWs (i. e. the sum of the objects observed in SEM weighted by their degree of coalescence) with a top facet of a given SEM intensity. The corresponding histograms of I_n are presented in Fig. 6, and compared to the histograms of NW heights in Fig. 2. Both types of histograms reveal similar trends which are related to the distribution of NW lengths: two populations of NWs are systematically observed, which we will refer to as *long* NWs and *short* NWs. These two populations are indistinguishable in the reference sample grown in a single step (Fig. 4c). The NW lengths of this reference sample are widely distributed and a population of long NWs cannot be evidenced. To further analyze the double step growth, we fitted the length distributions of the corresponding samples with two gaussian curves. The histograms of Fig. 2, obtained from cross-section views, are relevant to estimate the average length of the two populations

of NWs. Those of Fig. 6 are more adapted to evaluate their surface density. All these data are summarized in Tab. 1.

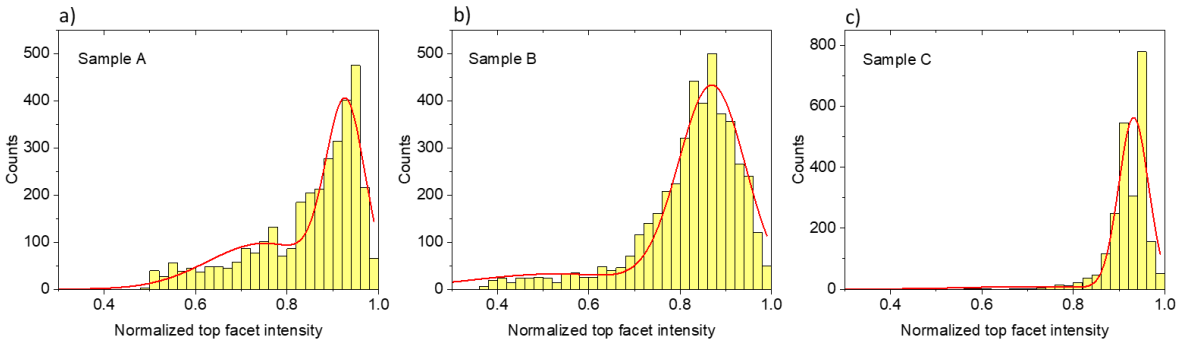

Figure 6: Histograms of normalized top facet SEM intensity for samples grown in a two-step process: a) sample A, $T_{g1} = 795°C$ and $T_{g2} = 815°C$; b) sample B, $T_{g1} = 795°C$ and $T_{g2} = 825°C$; c) sample C, $T_{g1} = 795°C$ and $T_{g2} = 835°C$.Red lines are fits by two gaussian curves.

Discussion

We first consider the total surface density of NWs. We obtain the following values: 3.7 x 10^{10} cm^{-2} for sample A, 3.9 x 10^{10} cm^{-2} for sample B, and 3.2 x 10^{10} cm^{-2} for sample C. For comparison, the NW density of the reference sample that has only undergone the first growth step ($t_1 = 35\ min$ at $T_{g1} = 795°C$) is 2.5 x 10^{10} cm^{-2}. Therefore, there is no clear trend emerging from the comparison of the samples, except that the two-step growth produces more NWs than the single-step growth. We must therefore conclude that new NWs have nucleated during the second growth step. We note, however, that the determination of these surface densities remains a difficult task since coalescence events bring a high degree of uncertainty to the absolute counting of individual NWs. Extracted densities are subject to large margins of error. A more significative trend is observed by comparing the ratios of the numbers of long and short NWs. The two types of histograms related to NW lengths agree on the fact that the population of short NWs gradually disappear by increasing the temperature of the second growth step. The long/short NW ratio is between 1 and 2 for $T_{g2} = 815°C$, between 2 and 5 for $T_{g2} = 825°C$ and is more than 10 at $T_{g2} = 835°C$. We now consider the peak length of the two NW populations. The heights of long and short NWs increase gradually with T_{g2}.

	Sample A $T_{g1} = 785°C$ $T_{g2} = 815°C$	Sample B $T_{g1} = 785°C$ $T_{g2} = 825°C$	Sample C $T_{g1} = 785°C$ $T_{g2} = 835°C$	Reference sample $T_{g1} = 785°C$
Total NW surface density from Fig. 6	$3.7\ x\ 10^{10} cm^{-2}$	$3.9\ x\ 10^{10} cm^{-2}$	$3.2\ x\ 10^{10} cm^{-2}$	$2.5\ x\ 10^{10} cm^{-2}$
Average length of long NWs from Fig. 2	$447\ nm$	$466\ nm$	$906\ nm$	$?\ nm$

Average length of short NWs from Fig. 2	$135\ nm$	$250\ nm$	$273\ nm$	
Population ratio long/short NWs from Fig. 2	1.8	2.0	11.9	–
Population ratio long/short NWs from Fig. 6	1.3	5.0	16.2	–

Table 1: Characteristics of the two populations of NWs observed by SEM cross-section and plane views.

Hence, our results clearly indicate that the two growth stages carried out at two different temperatures lead to two distinct NW populations. Growth temperature, T_g, has a major influence on NW nucleation and growth kinetics: we have shown that incubation time depends exponentially on T_g [9] and adatom surface diffusion is thermally activated. Therefore, it is very likely that the two populations of NWs are associated with the two stages of growth. The long NWs nucleated during the first growth step at $T_{g1} = 795°C$ and continued their growth during the second step. On the other hand, the shorter NWs nucleated during the second step at T_{g2}. Indeed, we know from our first series of experiments that nucleation is still possible at $815°C$. At this temperature and for a second step duration $t_2 = 90\ min$, nucleation is even highly probable since the duration t_2 is equal to the estimated incubation time. For $T_{g2} = 825°C$, the number of short NWs is still significant although reduced, indicating that even at this temperature, new GaN nuclei continue to form. For $T_{g2} = 835°C$, the population of short NWs is very small. This means that nucleation is almost suppressed at this temperature. Therefore, the growth conditions of sample C seem ideal to induce nucleation only during the first growth step, with a reduced incubation time, and to prolong the growth of already formed NWs during the second step without creation of new NWs. Moreover, high growth temperature is beneficial to the optical quality of the NWs [14].

We also observe that the elongation rate is increased at $T_{g2} = 835°C$ which produces the longest NWs of the sample series. The diffusion length of Ga adatoms on the NW sidewall facets has been estimated at 40–45 nm for temperatures between $780–800°C$ [18], [19]. At higher temperatures, diffusion is expected to increase, leading to a greater adatom current toward the top facet, which could explain the enhanced axial growth rate. At the same time, we have noticed that the radial growth rate also increases with T_{g2}. In fact, the adatom diffusion length remains shorter than the NW height, meaning that radial growth is still possible at high temperatures. The promotion of radial growth in sample C is likely due to more efficient diffusion of adatoms from the graphene substrate to the NW sidewalls at elevated temperatures. The quasi-absence of nucleation of new NWs at $835°C$ suggests that adatoms, which in samples A and B contributed to the formation of short NWs, were instead incorporated elsewhere in sample C, most likely along the NW sidewalls. In this sample, all incoming atoms fuel both axial and radial growth of NWs initiated during the first growth step. Notably, Table 1 indicates that the amount of material deposited as NWs is greater in sample C than in samples A and B. This discrepancy could be explained by the formation of a parasitic GaN deposit on the graphene surface surrounding the NWs in samples A and B during the second growth step. Such a parasitic layer has been identified in NW samples grown at $800°C$ (see supplementary information, Fig. S1d).

Another attractive feature of sample C is the narrow length distribution of long NWs, which can be seen on both histograms of Fig. 2 and Fig. 6. The standard deviations of the gaussian fits for long NW

distributions of Fig. 2 are $144\ nm$ for sample A, $128\ nm$ for sample B and $50\ nm$ for sample C. In summary, increasing the temperature of the second growth stage, T_{g2}, has two advantages: it stops the nucleation of new NWs and makes those already formed in the first stage more uniform in length. However, the phenomenon of coalescence which is very pronounced in sample C, is not favourable to our objectives. It is a source of structural defects which must be avoided. This leads us to the final part of this study where we apply the two-step growth procedure on patterned graphene substrates.

We have observed coalescence events in all our samples, including the reference sample (Fig. 4a). These coalescences which can start at the first growth step, are detrimental to the structural and optical quality of these objects. Indeed, in most cases, they generate extended defects such stacking faults and dislocations [20] as well as inhomogeneous strain [21]. To eliminate the coalescence, the graphene layer can be patterned into very small dots in order to organize the growth of single NWs at controlled location of the substrate surface. Using electron beam lithography to create graphene dot patterns, we have demonstrated that this approach can be successful if the diameter of the dots is small enough to prevent the nucleation of several NWs per dot [22], [23]. In the last part of this work, we apply our optimized two-step growth procedure to the growth of GaN NWs on patterned graphene.

To pattern the graphene patch, a negative resist (ma-N) was deposited onto the graphene surface before electron beam writing. The patterns consist of dots with diameters of 60 nm, 90 nm, and 120 nm, evenly spaced at 2.5 µm. After development, graphene was etched by oxygen plasma. Finally, the reticulated resist protecting the graphene dots was removed through successive solvent baths (acetone, isopropanol).

It has been reported that GaN nucleation on small graphene dots is more difficult than on large graphene patches [22], meaning that the incubation time lengthens below a critical pattern size. Fig. S5 (supplementary information) which shows a region of a sample with small dots patterned beside a large area of graphene, clearly illustrates this phenomenon. The NWs are much shorter on the small dots compared to the large graphene area.

Therefore, the two-step procedure is of particular interest for growth on small patterns. However, by keeping the first growth step at $795°C$, the incubation time on the small patterns still proved too long. For this reason, we slightly reduced T_{g1} to $790°C$. We tested three different values of t_1 for the first step duration, 25 min, 15 min and 10 min. For the second step, we used $T_{g2} = 835°C$ and $t_2 = 90\ min$ for the three samples. Fig. 7a shows an array of 60-nm-diameter graphene dots after the two-step growth with $t_1 = 25\ min$. NWs have developed both on dots, where all sites are occupied, and on SiO_2. This loss of selectivity is probably related to the slight decrease of T_{g1} that we found necessary for the small patterns.

The parasitic NWs (those on SiO_2) are much thinner and shorter than the NWs on the graphene dots. This means that growth on SiO_2 started later than on graphene, i. e. the nucleation barrier is still higher on SiO_2 than on graphene. Consequently, growth selectivity should improve by reducing t_1. This is indeed verified on the NW array grown with $t_1 = 15\ min$ (Fig. 7b). In this sample, the parasitic growth is significantly reduced while all the graphene dots are occupied, by single NWs mainly. For the third duration of the first growth step, $t_1 = 10\ min$, we did not observe any NW, on either SiO_2 or graphene.

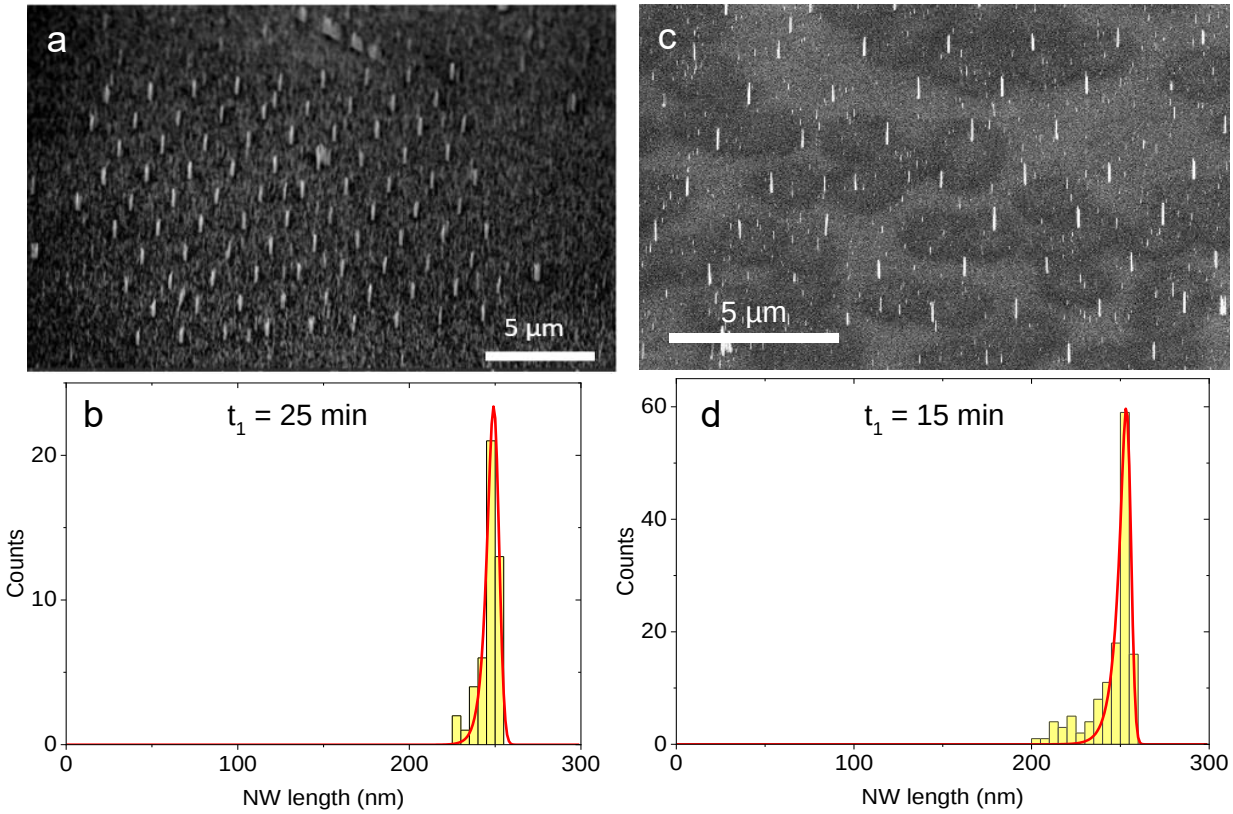

Figure 7: a, c) 45°-tilted SEM image of the GaN NW sample grown on patterned graphene with a double-step process: First step at $T_{g1} = 795°C$, $t_1 = 25\ min$ (a) or $15\ min$ (c), second step $t_2 = 90\ min$ at $T_{g2} = 835°C$; b, d) histogram of lengths for the NWs grown on the graphene dots (yellow bars) and fits of the distributions using the expression of ref [18] (red lines) for both t_1 durations.

We now consider the distributions of NW lengths in the two patterned samples where NWs were obtained. For both samples, the histograms (Fig. 7b and 7d) evidence a remarkable uniformity of length. To assess the advantage of the two-step growth process, we compare the present results to those of Morassi *et al.* where a single growth step on patterned graphene is used [18]. In this previous study, the NW length distributions were described with a model taking into account the incubation time, which was found to increase significantly for the smaller graphene dots. For 100-nm-diameter graphene dots, i. e. larger than in the present study, the mean length was $406\ nm$ with a standard deviation of $178\ nm$. We used the same expression to fit the distributions of Fig. 7. We obtain a mean length of $246\ nm$ with a standard deviation of 6.2 nm for $t_1 = 25\ min$ and a mean length of $245\ nm$ with a standard deviation of 12.2 nm for $t_1 = 15\ min$. These standard deviations represent 4.8 % and 2.5 % of the mean lengths respectively, while in the case of the study of Morassi *et al.*, this percentage was 44 %. We point out that these statistics only concern NWs that have grown on graphene dots patterned intentionally. This clearly demonstrate that the better uniformity of NW height that we observed for a two-step growth on a continuous sheet of graphene is also effective for organized arrays of graphene dots. However, a better uniformity was expected for the shorter t_1. We have no clear explanation for the moment as to why this is not the case. The parasitic growth on SiO_2 may play some role. The other important feature is the number of NWs per dots. We almost reach the ideal situation

where a single NW per dot is obtained. There is no empty dot and only very few dots 10% resulted in the growth of two NWs.

On the other hand, we were unable to completely suppress the parasitic growth on SiO_2 while maintaining the growth of NWs on graphene. The first solution is to increase T_{g1}, the counterpart being a longer incubation time and therefore a longer t_1. Another plausible reason for the parasitic growth could be related to a non-optimized lithography process leaving small residues of unwanted graphene outsides the dots. Further investigations are needed to verify this point. We also propose a solution to get rid of these parasitic NWs which are smaller and much thinner than the intended NWs. A short bath in a GaN wet etchant using a 5% diluted $S_2K_2O_8$ solution, followed by a 10% diluted KOH solution, and concluding with a rinse in DI water can be effective in eliminating the parasitic part while leaving the organized array practically unchanged. This has been successfully tested on one sample (Fig. 8). Such a sample would provide an excellent basis for epitaxial lateral overgrowth using a suitable technique, such as metalorganic vapor phase epitaxy (MOVPE) or hydride vapor phase epitaxy (HVPE), to produce an array of µm-sized and monocrystalline domains of GaN free of structural defects. Our next objective is to follow this approach to produce efficient micro-LEDs that can be easily transferred to a host substrate.

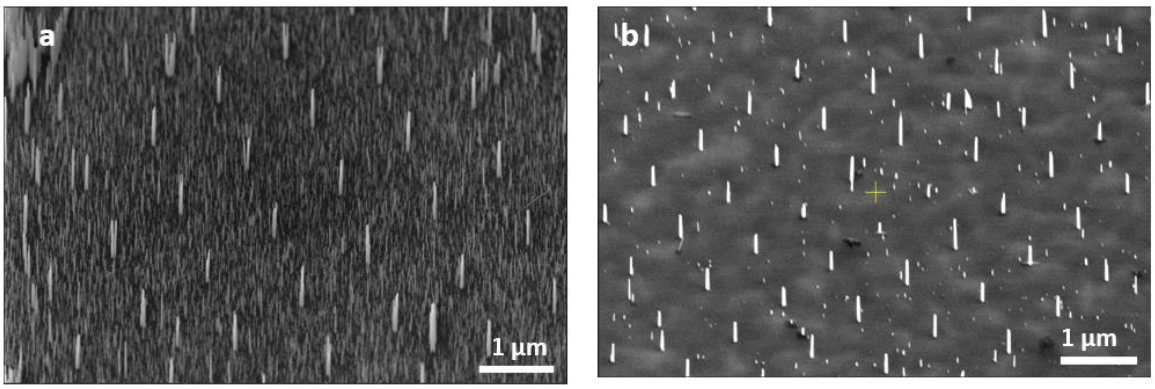

Figure 8: SEM images illustrating an attempt to eliminate by chemical etching the parasitic NWs grown on SiO_2 between the graphene patches of a patterned sample. a) before chemical etching; b) after chemical etching.

Summary and conclusions

In summary, we used a two-step MBE growth process to form GaN NWs on graphene with a reduced incubation time and a good height uniformity. The first step performed at 795°C instead of our usual temperature of 825°C has allowed us to shorten the incubation time from 90 min to 25 min. We have demonstrated that a temperature of at least 835°C must be used for the second step in order to avoid nucleation of new NWs during this next stage. This temperature also leads to an excellent uniformity of NW height. We applied this method on patterned graphene substrates and we obtained an array of homogeneous and organized GaN NWs. Such a sample can be used as seeds to form GaN micro-domains by lateral overgrowth. These domains could be defect-free and would represent an assembly of micro-substrates of high structural quality on which micro-LEDs could be fabricated.

Acknowledgments

This research was supported by the French National Research FLAGG Project (Grant ANR-21-CE24-0017-01), by LABEX GANEXT project LEDFLEX and by the French RENATECH network. The work was partly performed in the C2N nanotechnology platform. The authors acknowledge the engineers of this platform for their assistance with specific technological steps and for training our students.

Bibliography

[1] Li S and Waag A 2012 GaN based nanorods for solid state lighting *J. Appl. Phys.* **111** 071101

[2] Monemar B, Ohlsson B J, Gardner N F and Samuelson L 2016 Nanowire-Based Visible Light Emitters, Present Status and Outlook *Semiconductors and Semimetals* **94** 227-271

[3] Kuykendall T, Pauzauskie P, Lee S, Zhang Y, Goldberger J and Yang P 2003 Metalorganic chemical vapor deposition route to GaN nanowires with triangular cross sections *Nano Lett.* **3**(8) 1063-1066

[4] Seryogin G, Shalish I, Moberlychan W and Narayanamurti V 2005 Catalytic hydride vapour phase epitaxy growth of GaN nanowires *Nanotechnology* **16** 2342

[5] Calleja E, Sánchez-García M A, Sánchez F J, Calle F, Naranjo F B, Muñoz E, Jahn U and Ploog K 2000 Luminescence properties and defects in GaN nanocolumns grown by molecular beam epitaxy *Phys. Rev. B - Condens. Matter Mater. Phys.* **62** 16826

[6] Consonni V, Knelangen M, Geelhaar L, Trampert A and Riechert H 2010 Nucleation mechanisms of epitaxial GaN nanowires: Origin of their self-induced formation and initial radius Phys. Rev. B - Condens. Matter Mater. Phys. **81** 085310

[7] Consonni V, Trampert A, Geelhaar L and Riechert H 2011 Physical origin of the incubation time of self-induced GaN nanowires *Appl. Phys. Lett.* **99** 033102

[8] Zettler J K, Corfdir P, Geelhaar L, Riechert H, Brandt O and Fernández-Garrido S 2015 Improved control over spontaneously formed GaN nanowires in molecular beam epitaxy using a two-step growth process *Nanotechnology* **26** 445604

[9] Sobanska M, Klosek K, Borysiuk J, Kret S, Tchutchulasvili G, Gieraltowska S and Zytkiewicz Z R 2014 Enhanced catalyst-free nucleation of GaN nanowires on amorphous Al2O3by plasma-assisted molecular beam epitaxy *J. Appl. Phys.* **115** 043517

[10] Sobanska M, Dubrovskii V G, Tchutchulashvili G, Klosek K and Zytkiewicz Z R 2016 Analysis of Incubation Times for the Self-Induced Formation of GaN Nanowires: Influence of the Substrate on the Nucleation Mechanism *Cryst. Growth Des.* **16** (12) 7205–7211

[11] Barbier C, Largeau L, Gogneau N, Travers L, David C, Madouri A, Tamsaout D, Girard J C, Rodary G, Montigaud H, Durand C, Tchernycheva M, Glas F and Harmand J C 2023 What Triggers Epitaxial Growth of GaN on Graphene? *Cryst. Growth Des.* **23** (9) 6517–6525

[12] Chèze C, Geelhaar L, Brandt O, Weber W M, Riechert H, Münch S, Rothemund R, Reitzenstein S, Forchel A, Kehagias T, Komninou P, Dimitrakopulos G P and Karakostas T 2010 Direct comparison of catalyst-free and catalyst-induced GaN nanowires *Nano Res.* **3** 528–536

[13] Fernández-Garrido S, Zettler J K, Geelhaar L and Brandt O 2015 Monitoring the formation of nanowires by line-of-sight quadrupole mass spectrometry: A comprehensive description of the temporal evolution of GaN nanowire ensembles *Nano Lett.* **15** (3) 1930–1937

[14] Kumaresan V, Largeau L, Madouri A, Glas F, Zhang H, Oehler F, Cavanna A, Babichev A, Travers L, Gogneau N, Tchernycheva M and Harmand J C 2016 Epitaxy of GaN Nanowires on Graphene *Nano Lett.* **16** (8) 4895–4902

[15] Kumaresan V, Largeau L, Oehler F, Zhang H, Mauguin O, Glas F, Gogneau N, Tchernycheva M and Harmand J-C 2016 Self-induced growth of vertical GaN nanowires on silica *Nanotechnology* **27** 135602

[16] Zettler J K, Hauswald C, Corfdir P, Musolino M, Geelhaar L, Riechert H, Brandt O and Fernández-Garrido S 2015 High-Temperature Growth of GaN Nanowires by Molecular Beam Epitaxy: Toward the Material Quality of Bulk GaN *Cryst. Growth Des.* **15** (8) 4104–4109

[17] Brandt O, Fernández-Garrido S, Zettler J K, Luna E, Jahn U, Chèze C and Kaganer V M 2014 Statistical analysis of the shape of one-dimensional nanostructures: Determining the coalescence degree of spontaneously formed GaN nanowires *Cryst. Growth Des.* **14** (5) 2246–225

[18] Debnath R K, Meijers R, Richter T, Stoica T, Calarco R and Lüth H 2007 Mechanism of molecular beam epitaxy growth of GaN nanowires on Si(111) *Appl. Phys. Lett.* **90**, 123117

[19] Galopin E, Largeau L, Patriarche G, Travers L, Glas F and Harmand J C 2011 Morphology of self-catalyzed GaN nanowires and chronology of their formation by molecular beam epitaxy *Nanotechnology* **22** 245606

[20] Grossklaus K A, Banerjee A, Jahangir S, Bhattacharya P and Millunchick J M 2013 Misorientation defects in coalesced self-catalyzed GaN nanowires *J. Cryst. Growth*

[21] Fernández-Garrido S, Kaganer V M, Hauswald C, Jenichen B, Ramsteiner M, Consonni V, Geelhaar L and Brandt O 2014 Correlation between the structural and optical properties of spontaneously formed GaN nanowires: A quantitative evaluation of the impact of nanowire coalescence *Nanotechnology* **25** 455702

[22] Morassi M, Guan N, Dubrovskii V G, Berdnikov Y, Barbier C, Mancini L, Largeau L, Babichev A V, Kumaresan V, Julien F H, Travers L, Gogneau N, Harmand J-C and Tchernycheva M 2020 Selective Area Growth of GaN Nanowires on Graphene Nanodots *Cryst. Growth Des.* **20** (2) 552–559

[23] Mancini L, Morassi M, Sinito C, Brandt O, Geelhaar L, Song H-G, Cho Y-H, Guan N, Cavanna A, Njeim J, Madouri A, Barbier C, Largeau L, Babichev A, Julien F H, Travers L, Oehler F, Gogneau N, Harmand J-C and Tchernycheva M 2019 Optical properties of GaN nanowires grown on chemical vapor deposited-graphene *Nanotechnology* **30** 214005

Supplementary information

TEM observations

We observed GaN NWs grown on graphene by TEM and STEM. Figure S1 shows the vertical alignment of their c axis. The diffraction pattern obtained on a NW ensemble indicates that they all have the same in plane orientation. The absence of Ga droplet at the top of the NWs suggests that they are formed by a vapor-solid mechanism. STEM analysis also revealed the presence of a parasitic layer surrounding the NWs (Fig. S1d) and identified as GaN by energy dispersion X-ray spectroscopy for samples grown at 800°C.

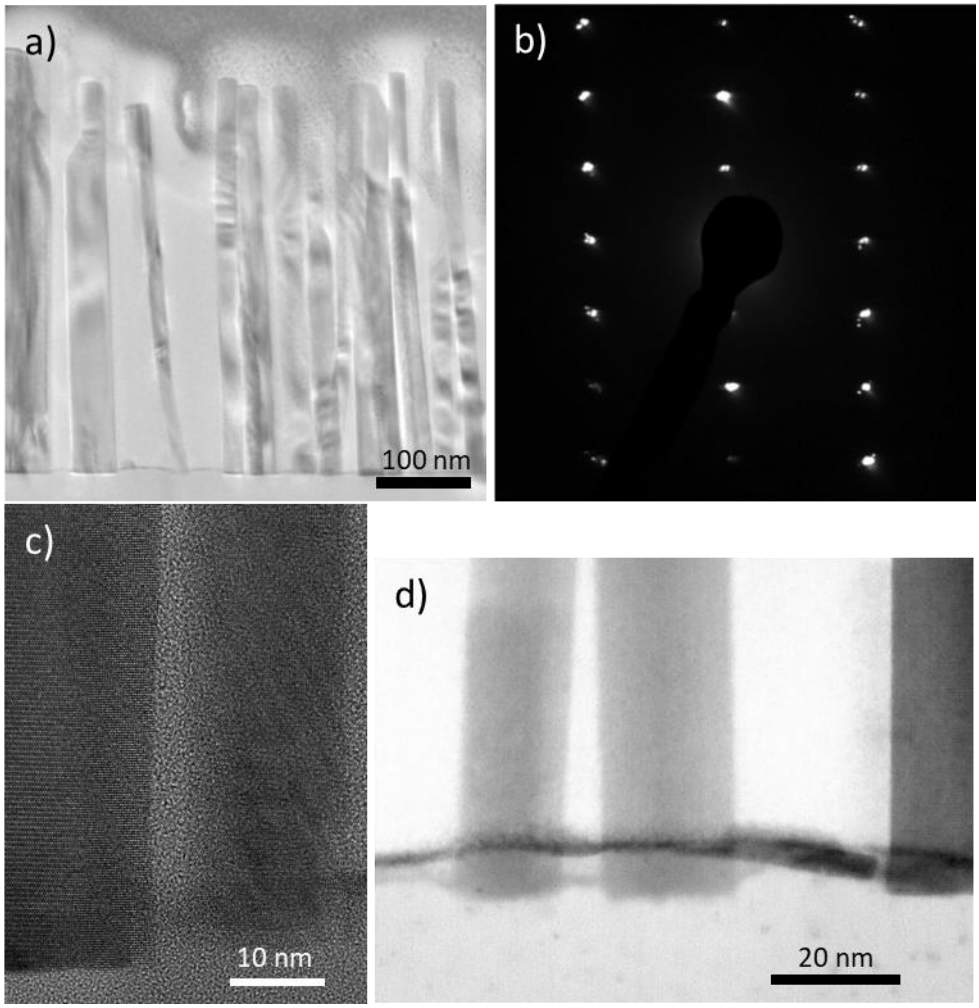

Figure S1: TEM analysis of GaN NWs grown on graphene. a) TEM cross-section view of an ensemble of vertically aligned NWs and b) the corresponding diffraction pattern revealing their hexagonal structure and their orientation along the c axis; c) high-resolution TEM at the bottom of two NWs; d) Cs-corrected bright-field STEM at the bottom of NWs showing the presence of a parasitic layer identified as GaN by energy dispersion X-ray spectroscopy (not shown).

Graphene transfer and patterning

The graphene film is grown by chemical vapor deposition on copper. Then the graphene is separated from copper by wet etching and transferred on a silica layer obtained by thermal oxidation of a Si (100) substrate. The result is shown in Fig. S2a). Most of the area consists of a single monolayer of graphene but the dark spots indicate nucleation points of a second graphene monolayer. The dark filaments are folds of graphene formed during the transfer process. To organize the growth of NWs at controlled location of the substrate surface, the graphene layer is patterned into small dots using electron beam lithography (Fig S2b). A negative resist (ma-N) is deposited onto the graphene surface before electron beam writing. After development, graphene was etched by oxygen plasma and the reticulated resist was removed through successive solvent baths.

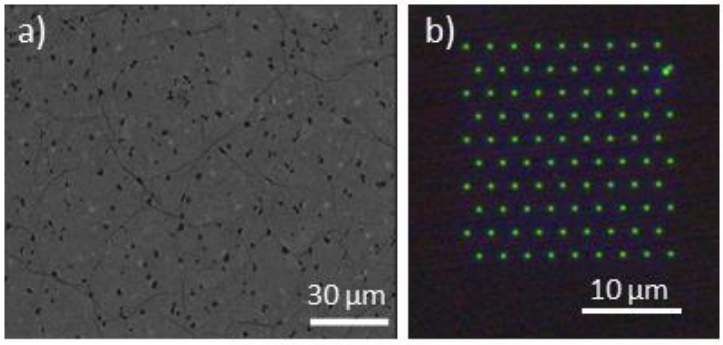

Figure S2: a) SEM image of a graphene film transferred onto silica. b) Optical microscopy of a graphene film after e-beam patterning.

Interpretation of the SEM contrast of the NW top facets

The SEM intensity of the top facet of a particular NW depends on its height. This is due firstly to the out-of-optical-axis configuration of the through lens detector that we use which gives a topographical contrast. Then, it is also due to the interaction volume of the primary electron beam within each NW. We used an incident energy of 10 keV for which the excitation or generation depth is estimated between 420 nm [S1] and 805 nm [S2], the latter value being close to experimental results [S3]. Therefore, we can consider that at this incident energy, the whole volume of each NW is excited by the electron beam. Consequently, the interaction volume is smaller for the shorter NWs, they emit less secondary electrons and their top facet appears less bright on the SEM images. To confirm that the contrast is related to the change of interaction volume for NWs of different height, we observed a NW sample under various incident energies of the primary electron beam. We varied the acceleration or deceleration voltage. For energies lower than 10 keV, the contrast of the top facets of NWs of different length weakens. In conclusion, the distribution of the top facet intensities contains information on the NW length distribution.

Coalescence and circularity

To estimate the number on NWs in a bunch of coalesced NWs, we used the circularity C of the top facet of the bunch (see ref). For a given interval of circularity, we associate a given number of NWs. To define a simple rule for this correspondence, we consider series of n connected regular hexagons with edges of length a. In the first series, neighboring hexagons have one common edge. The total

perimeter evolves as $\big(10+4(n-2)\big)a$, the total area is $\frac{3\sqrt{3}}{2}na^2$ and the circularity is $\frac{3\sqrt{3}\pi n}{2(2n+1)^2}$. In the second series, we assume a longitudinal smoothening by radial growth which gives a straight connection between the individual wires. The perimeter is $2\left(3+\sqrt{3}(n-1)\right)a$, the area is $\frac{\sqrt{3}}{2}(4n-1)a^2$ and their circularity is $\frac{\sqrt{3}\pi(4n-1)}{2\left(3+\sqrt{3}(n-1)\right)^2}$. To associate the number of NWs to a bundle of given circularity, we use the average value of the $C(n)$ functions of the two series, as defined in Table 1. We check that the obtained value is consistent with the total area of the bundle top facet (i. e. equal to n times the average area of a single NW, within a factor of two). If not, we apply a criterion related to the facet area.

Number of hexagons	Circularity of series 1	Circularity of series 2	Average value	Applied rule
1	0.907	0.907	0.907	$1 < C < 0.752$
2	0.851	0.653	0.752	$0.752 < C < 0.608$
3	0.716	0.500	0.608	$0.608 < C < 0.505$
4	0.608	0.403	0.505	$0.505 < C < 0.431$
5	0.524	0.337	0.431	$0.431 < C < 0.375$
6	0.460	0.290	0.375	$0.375 < C < 0.332$
7	0.410	0.254	0.332	$0.332 < C < 0.297$
8	0.369	0.226	0.297	$0.297 < C < 0.269$
9	0.335	0.203	0.269	$0.246 < C < 0.375$
10	0.307	0.185	0.246	$0.246 < C < 0.226$

Table S1: Circularities of the two series of bundles of hexagons shown in Fig. S1 and the rule applied to analyze the SEM top views.

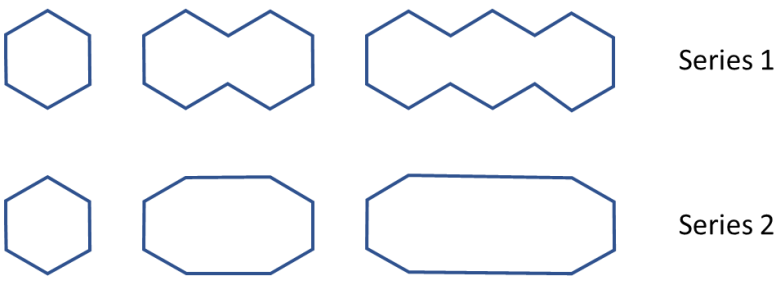

Figure S3: Sketch of the two series of connected hexagons for which the $C(n)$ function is considered.

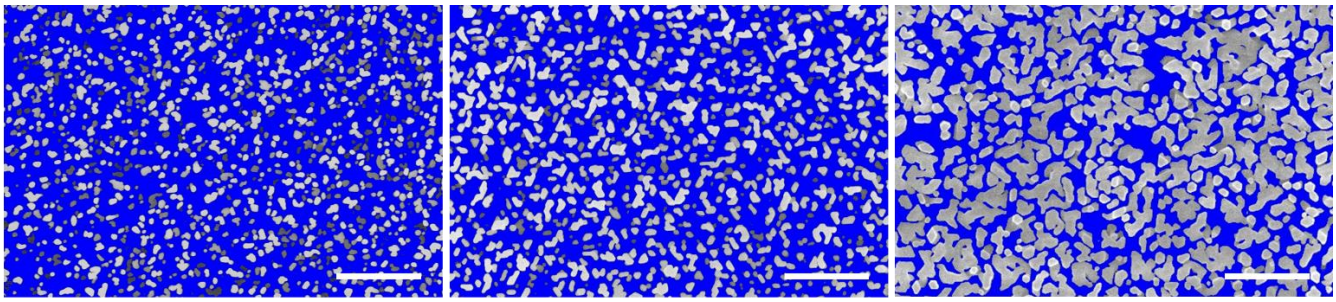

Figure S4: SEM top views of the three samples grown with a double-step process after adjusting the threshold.

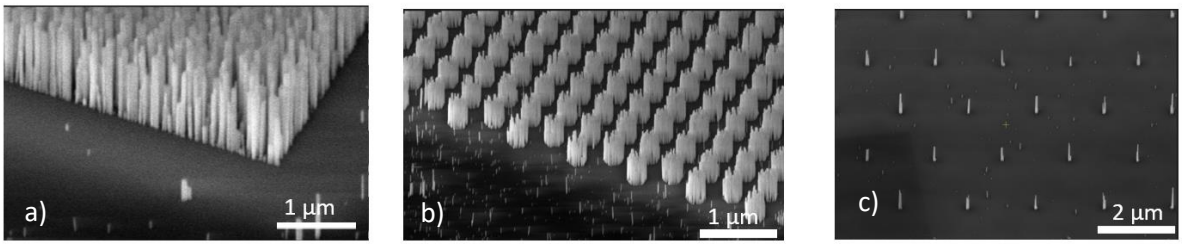

Figure S5: SEM images of the GaN NW sample on patterned graphene grown at Ts of 815°C for 4 hours tilted at 45° (a) on micrometer-sizes patterned graphene markers (b) hexagonal dot of d=250 nm (c) hexagonal dot of d=60 nm.

References

[S1] Everhart T E and Hoff P H 1971 Determination of kilovolt electron energy dissipation vs penetration distance in solid materials *J. Appl. Phys.* **42** 5837-5846

[S2] Kanaya K and Okayama S 1972 Penetration and energy-loss theory of electrons in solid targets *J. Phys. D : Appl. Phys.* **5** 43

[S3] Yacobi B G and Holt D B 1986 Cathodoluminescence scanning electron microscopy of semiconductors *J. Appl. Phys.* **59** R1-R24